Twisting a Cylindrical Sheet Makes it a Tunable Locking Material

Pan Dong[®], ^{1,2} Mengfei He[®], ^{1,2} Nathan C. Keim[®], ^{3,*} and Joseph D. Paulsen[®], ^{1,2}†

¹Department of Physics, Syracuse University, Syracuse, New York 13244, USA

²BioInspired Syracuse: Institute for Material and Living Systems, Syracuse University, Syracuse, New York 13244, USA

³Department of Physics, Pennsylvania State University, University Park, Pennsylvania 16802, USA

(Received 14 March 2023; accepted 31 August 2023; published 2 October 2023)

A buckled sheet offers a reservoir of material that can be unfurled at a later time. For sufficiently thin yet stiff materials, this geometric process has a striking mechanical feature: when the slack runs out, the material locks to further extension. Here, we establish a simple route to a tunable locking material: a system with an interval where it is freely deformable under a given deformation mode, and where the endpoints of this interval can be changed continuously over a wide range. We demonstrate this type of mechanical response in a thin sheet formed into a cylindrical shell and subjected to axial twist and compression, and we rationalize our results with a simple geometric model.

DOI: 10.1103/PhysRevLett.131.148201

When a thin material is compressed, small-scale wrinkles and folds may form to collect excess length. Looking at this process in reverse, buckled microstructures can be thought of as a reservoir of material that can be deployed at a later time. This strategy is exploited in designed structures ranging from the common umbrella to inflatable satellites [1,2]. It is also harnessed in nature, for instance in the capture thread of the orb-weaving spider [3,4] and in rabbit mesentery [5]. The process of buckling and deploying material length is rich in its geometric aspects [6], and it also has a striking mechanical feature: a wrinkled sheet has approximately no resistance to extension until it becomes taut, at which point the force to stretch the system further rapidly increases [Fig. 1(c)]. This mechanical response has been idealized in a theory of so-called "locking materials" [7,8].

Here, we establish a simple route to a *tunable* locking material: a system with an interval where it is freely deformable, and where the endpoints of this interval can be changed continuously over a wide range. We demonstrate this type of mechanical response in a thin cylindrical sheet subjected to axial twist and compression. Our measurements show that this system is soft to twisting up to a threshold "locking angle" φ_{ℓ} . By adapting the basic physical picture of tension field theory [9–12] into simple length-preserving arguments, we predict the locking angle as a function of a small set of geometric parameters. We identify a universal phase boundary between the soft

Published by the American Physical Society under the terms of the Creative Commons Attribution 4.0 International license. Further distribution of this work must maintain attribution to the author(s) and the published article's title, journal citation, and DOI. deformations facilitated by buckling and the stiff response where the system becomes taut, in agreement with our experiments. These results show how a material's locking position can be tuned *in situ*, which could find use in applications where a reprogrammable mechanical response is desired [13].

The phenomenon we study is shown in Fig. 1. Here, a rectangular mylar sheet (thickness $t = 6.5 \mu m$, Young's modulus E = 3.4 GPa) has been curved into a cylindrical shell by gluing two of its edges to rigid rings of radius R = 9.5 mm, which are mounted in a rheometer (Anton Paar MCR 302) for mechanical testing. Undeformed, the cylinder strongly resists extension, but will readily buckle and wrinkle under compression. Starting from an initial height of H = 26.9 mm, the cylinder is axially compressed to a height h = 22.2 mm so that it buckles into a loosely crumpled configuration [Fig. 1(a)]. Then, we slowly rotate the top ring. When the magnitude of the rotation angle φ reaches approximately 81°, we witness two striking events at once: (i) the complex crumpled state gives way to regular wrinkles, and (ii) the magnitude of the torque on the top ring begins to increase dramatically [Fig. 1(b)]. Performing this deformation cyclically reveals that these mechanical measurements and morphological transitions are repeatable.

The normal force on the top ring during the experiment also shows a dramatic increase in magnitude at the same angle φ_{ℓ} , as we show in Fig. 1(c). The wrinkled morphology of Fig. 1(a) shows why the two signals are linked: stresses are transmitted between the bottom and top rings along the wrinkle crests and troughs, which are tilted with respect to the vertical axis. Thus, we may use the normal force as a secondary signal to measure φ_{ℓ} .

Geometric model.—To understand the emergence of ordered wrinkles at a qualitative level, we imagine that

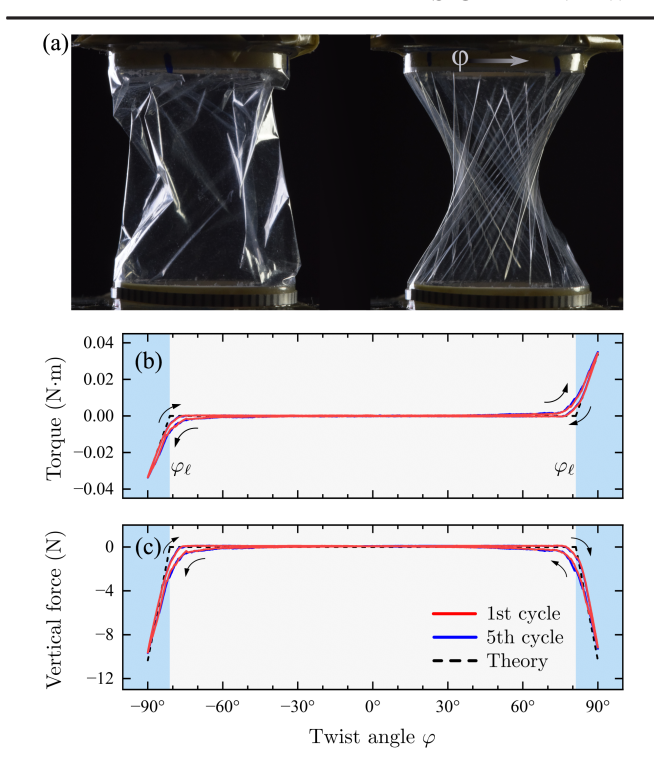


FIG. 1. Morphology and mechanics of a twisted cylindrical sheet. (a) A 6 µm thick shell of height H=26.9 mm and radius R=9.5 mm is mounted between parallel plates, compressed axially and then twisted. At a threshold twist angle, the shell transitions from a disordered buckled state to an ordered wrinkled state. Left: $\varphi=0$. Right: $\varphi=90^\circ$. (b),(c) Torque and vertical force on the top plate as such a cylinder is twisted cyclically between $\pm 90^\circ$ at constant separation (h=22.2 mm). The data rapidly increase in magnitude at the "locking angle" φ_ℓ . Our model predicts $\varphi_\ell=81^\circ$ for this shell [see Eq. (1)]. Dashed lines: predicted response past φ_ℓ (see SM and text).

the cylinder of initial height H is constructed of many vertical "ropes," which are inextensible yet have zero resistance to bending. When the cylinder is compressed to a smaller height h, these ropes buckle to collect the extra slack along their length. This buckling of the ropes serves as a reservoir of material that allows the cylinder to then be twisted by φ , until at some crucial angle φ_{ℓ} the slack runs out and the ropes become taut. The same picture holds if the initial direction of the ropes is skew, forming a set of geodesics that can be characterized by an offset angle θ at the cylindrical surface [see the segment \widehat{AB} in Fig. 2(a)]. As we will now show, there is a precise θ of the tilted ropes that forms the strongest constraint to the rotation. It is the geometric selection of θ that determines the locking angle φ_{ℓ} and the final orientation α of the wrinkles for the buckled configuration.

The key geometric observation is that the initial length of the rope $\widehat{AB} = \sqrt{H^2 + R^2\theta^2}$, must match the final length of the rope $\overline{A'B} = \sqrt{h^2 + 2R^2 - 2R^2\cos(\theta + \varphi)}$ at the point the system becomes taut. Equating these two and

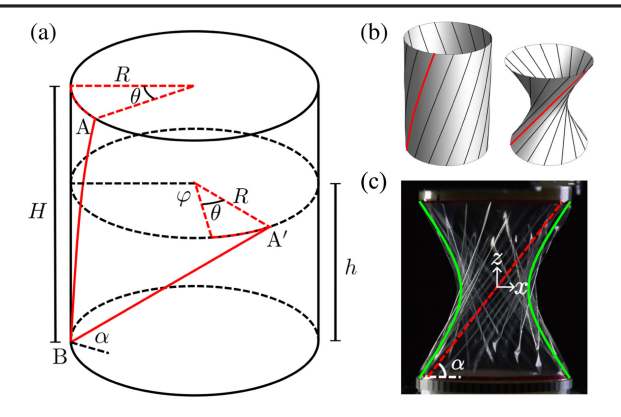


FIG. 2. Geometric idealization for compressing and twisting an inextensible cylindrical shell. (a) A cylindrical shell with an initial height H is compressed to a final height h and then twisted by φ . In this process, a geodesic AB, represented by the offset angle θ , is mapped onto a straight line A'B. Finding the largest allowed twist φ_{ℓ} that does not stretch the material between any two points amounts to identifying the most constraining θ that gives the least amount of twist while preserving the length AB = A'B. (b) An undeformed cylindrical shell and its idealized gross shape after compression and twist, showing the corresponding geodesics preserving the length. (c) Shape of a locked cylinder ($\varphi = \varphi_{\ell}$) with C = 0.64 and $\varphi = 1.42$. Green curves: hyperbola given by Eq. (3) in the marked x - z coordinate system. Red line: asymptote of the hyperbola, which matches the wrinkle angle α .

introducing a dimensionless compression parameter and a dimensionless aspect ratio,

$$C \equiv (H^2 - h^2)/(2R)^2$$
$$\rho \equiv H/(2R),$$

we obtain $1 - \theta^2/2 - \cos(\theta + \varphi) = 2C$. To see which θ poses the strongest constraint to rotation, we seek the value of θ for which φ is minimized; physically this corresponds to finding the set of lines in the undeformed cylindrical shell that become taut first, as the compressed shell is gradually twisted. The amount of twist φ_{ℓ} that locks the system is thus:

$$\varphi_{\ell} \equiv \min_{\theta} \{ \varphi(\theta) \}$$

$$= -2\sqrt{\sqrt{C} - C} + \cos^{-1} \left(1 - 2\sqrt{C} \right). \tag{1}$$

This minimum φ occurs at $\theta_m = 2\sqrt{\sqrt{C} - C}$, which identifies the material lines in the undeformed cylinder that lock the system.

To help visualize this picture, Fig. 2(b) is an illustration of these material lines (black helices wrapping the cylinder), and their taut counterparts in the compressed, twisted shell at φ_{ℓ} . Each taut line makes an angle α with the horizontal. To obtain an expression for α , we use the geometry in Fig. 2(a) to express α in terms of $\varphi_{\ell} + \theta_m$, h,

and R. Applying the definitions of the compression parameter C and the aspect ratio ρ , we find

$$\alpha = \tan^{-1} \sqrt{\frac{\rho^2 - C}{\sqrt{C}}}. (2)$$

We may also use these geometric arguments to obtain the overall shape of the shell at φ_{ℓ} (neglecting the wrinkly undulations). Because each point on the locked shell belongs to one taut line, the overall shape is given by sweeping the straight line $\overline{A'B}$ in Fig. 2(a) about the axis of the cylinder. This surface thus generated is a hyperboloid of revolution [14,15], and its side profile is the hyperbola

$$x^2/a^2 - z^2/c^2 = R^2. (3)$$

Remarkably, the angle α of the line $\overline{A'B}$ is equal to the angle of the asymptote of the side-view profile [16], $z = (c/a) \cdot x = \tan \alpha \cdot x$. This allows us to express the ratio c/a in terms of ρ and C, through Eq. (2). To obtain c and a, we combine this result with Eq. (3) applied to the top boundary of the cylinder, $R^2/a^2 - h^2/(4c^2) = R^2$. Solving these two equations gives: $a^2 = 1 - \sqrt{C}$ and $c^2 = (\rho^2 - C)(1 - \sqrt{C})/\sqrt{C}$.

As a first test of our model, we compare these predictions with the cylinder from Figs. 1 and 2(c) with C=0.64 and $\rho=1.42$. Figure 2(c) shows the predicted hyperbolic shape, which is in reasonable agreement with the observed side-view profile, allowing for the finite-amplitude wrinkles that protrude from the hyperboloid shape, and that we neglect in the model. We also show the asymptote, which agrees with the orientation of the wrinkles passing through the center of the shell in the plane normal to the line of sight. Finally, the locking angle predicted by Eq. (1), $\varphi_{\ell}=81^{\circ}$, is in reasonable agreement with the location of the rapid increase in magnitude of the force and torque curves in Figs. 1(b) and 1(c).

Tunability.—A more comprehensive test of the predicted locking angle involves probing it as a function of the axial compression. Indeed, our geometric model predicts the phase boundary between relaxed and stretched states, and we may plot Eq. (1) on a phase diagram as in Fig. 3. At a given axial compression, C, the shell is soft to rotation within the interval $|\varphi| < \varphi_{\ell}$. Figure 3 shows that the width of this interval can be tuned on demand between 0 and 360°.

To test this picture, we designed a protocol to trace out the phase boundary in a single experiment. We twist the cylinder back and forth between $\pm 360^{\circ}$ at a constant rate, keeping a small separation force -0.5 N between the top and bottom plates of the cylinder. The exact value of this force is not important, but it must be small enough to avoid tearing the material, and large enough to activate relaxations of the wrinkle pattern toward the lowest-energy

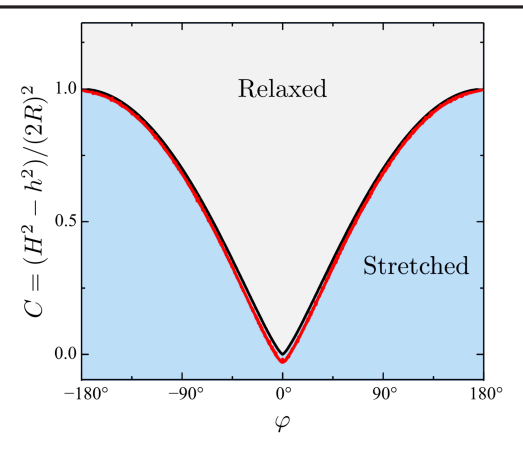


FIG. 3. Phase diagram of a cylindrical shell subjected to axial compression C and twist φ . Modeling the system as a material that can compress but not stretch makes every point in the "relaxed" phase accessible (up to the horizontal line $C=\rho^2$ that corresponds to full compression with h=0). Our geometric model predicts the phase boundary where the system locks and becomes taut [Eq. (1), black line]. Red curve: experiment with a 1.5 μ m thick shell with R=9.5 mm and H=26.9 mm, cycling between $\varphi=\pm180^\circ$ at a constant rate while applying a small lifting force F=-0.5 N at the top boundary. The data are in good agreement with our model that has no free parameters. The small discrepancy around $\varphi=0$ is due to finite stretching; see SM [17].

ordered state [see Supplemental Material (SM) [17]]. This force causes the cylinder to gradually decrease or increase its height in response to the continuous twisting, maintaining a taut configuration. In this process we track the twist angle φ and the resulting compression C, calculated from the initial height H and the adapted height h. Figure 3 shows an excellent match between the curve traced out by the test cycle and the relation from Eq. (1), within the working regime $|\varphi| < 180^{\circ}$ of our geometric model. This is notable given that our model does not include the bending or stretching moduli of the sheet, and it does not take into account the finite size of the wrinkles or the boundary layer where the wrinkle amplitude decays to zero at the clamped boundaries.

There is another striking simplicity of the behavior: Equation (1) predicts that the phase diagram is independent of the initial shape of the cylinder— ρ is absent from Eq. (1) and the phase diagram axes (Fig. 3). To further demonstrate this universality, we perform a new experiment with a cylinder of aspect ratio $\rho=0.79$ and compare it to the earlier test with $\rho=1.42$. Figure 4(a) shows that the curves followed by the slender and squat cylinders both fall along our model prediction [Eq. (1)].

The fates of the two cylinders at their limits of rotation, however, are different. When the slender cylinder ($\rho = 1.42$) is twisted toward 180°, a tight waist appears that contracts to a small size to form a double-cone structure [Figs. 4(b)–4(e)]. Indeed, at $\varphi_{\ell} = 180^{\circ}$ (C = 1), our geometric argument predicts that all lines of tension

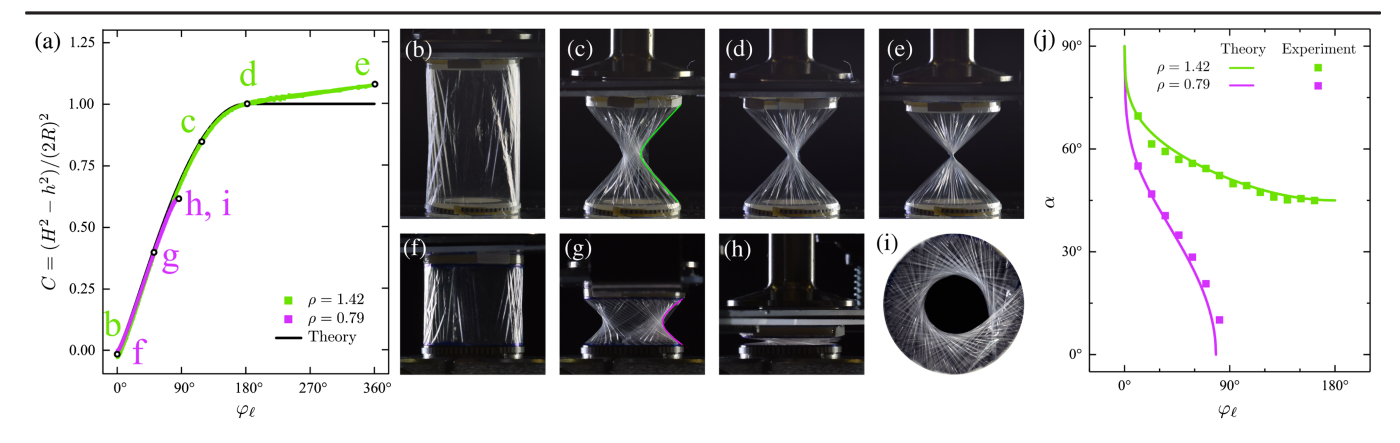


FIG. 4. Effects of the aspect ratio ρ of the cylinder. (a) Locking curves for two 1.5- μ m-thick cylindrical shells with the same radius R=9.52 mm but different heights, twisted from 0° to 360° at a constant rate while applying a small lifting force F=-0.5 N at the top boundary. Green: H=26.9 mm, $\rho=1.42$. Magenta: H=15.0 mm, $\rho=0.79$. (b)–(e) Side-view images of the slender shell ($\rho=1.42$) at $\varphi=0^\circ$, 120°, 180°, 360°. (f)–(h) Side-view images of the squat shell ($\rho=0.79$) at $\varphi=0^\circ$, 52°, 87°. (i) Bottom-view image of the configuration of (h). (j) Markers: observed angle of wrinkles with respect to the vertical direction, versus the locking angle φ_{ℓ} , for the two cylinders. Curves: Eq. (2) for the angle of the lines of tension.

[represented by $\overline{A'B}$ in Fig. 2(a)] simultaneously pass through the center of the cylinder. A simple way for our model to handle this self-contact is for the lines of tension to curl around one another at the apex of the double cone, leaving h fixed even as the twist exceeds 180°. This idealized behavior is represented by the horizontal line C=1 for $\varphi_{\ell}>180^{\circ}$ in Fig. 4(a). The torque is zero along this line as the lines of tension have lost their azimuthal component. In the experiment, the finite thickness of the shell causes a finite-sized waist to form, so that the dimensionless compression C rises slowly for $\varphi_{\ell}>180^{\circ}$, and a small torque is observed.

On the other hand, a squat cylinder with $\rho = H/(2R) < 1$ cannot be twisted up to $\varphi = 180^\circ$. At $\varphi_\ell = -2\sqrt{\rho - \rho^2} + \cos^{-1}(1-2\rho) < 180^\circ$, h=0 and the top and bottom come into contact as shown in the sequence of images in Figs. 4(f)–4(h) for an experimental realization with $\rho = 0.79$. This deformation results in a finite throat size, seen in the bottom view of Fig. 4(i). As a consequence of this evolution, a squat cylinder never loses its locking ability.

The orientation of the lines of stress also depends on the aspect ratio ρ . Figure 4(j) shows the measured wrinkle tilt α for the same two cylinders but different aspect ratios ($\rho = 1.42$ and 0.79) at a series of locked configurations. For the slender cylinder ($\rho > 1$), the wrinkle direction plateaus to the double-cone limit at large twist. For the squat cylinder ($\rho < 1$), the wrinkles become more and more skew until they lay down completely as the shell flattens into a wrinkled annulus. Both trends are captured accurately by our geometric prediction, Eq. (2).

Stiffness at locking.—To understand the stiffness that the system presents as it locks, we extend our geometric model to infinitesimal rotations beyond locking, where we expect that the configuration of the wrinkles remains fixed while

the material is stretched along their crests and troughs. In the SM [17] we show how the material strain may be computed using Eqs. (1)–(3) and then converted into the vertical force and torque on the top plate. Figures 1(b) and 1(c) show that these predictions with no free parameters quantitatively capture the data beyond locking.

Discussion.—We have shown how a thin cylindrical shell can be manipulated to give rise to a tunable locking behavior, where the torque and force dramatically increase beyond the locking angles $\pm \varphi_{\ell}$. Beyond the locking point the material stretches, so that in the blue shaded region of Fig. 3 the system acts as an extensional or torsional spring [18] with a stiffness that we have rationalized. Our geometric arguments show how φ_{ℓ} can be set on demand over a wide range—anywhere from 0° to 180°—and our results apply to sufficiently thin cylindrical shells of any aspect ratio. This behavior is amenable to applications, as the system is lightweight and relies on a low-cost film.

At a twist angle of 180°, our purely geometric arguments show that the sheet must make contact with itself. As we approach this angle from below, the waist of the sheet approaches zero radius, wrinkles become more prevalent, and the sheet's finite bending modulus and thickness play a role, so that the experimental data begin to deviate from our model. Eventually a tight bundle forms where the material twists around itself in a neck that joins two wrinkled cones—reminiscent of a twisted candy wrapper, sausage casing, party balloon [19], or towel. An understanding of this bundle must take into account the finite thickness of the film, the friction of self-contact, and the geometric problem of packing the sheet into a small cross section [20].

Our results suggest a fascinating landscape of configurations for the sheet. In our idealized model, each point on the phase boundary corresponds to a unique configuration of the sheet, where uniform wrinkles orient at an angle α

around a hyperbolic profile. This is reflected in our experiments as a robust and repeatable ordered response at the phase boundary, although the precise placement of wrinkles can differ in each realization. Slightly away from the phase boundary, the number of possible states expands dramatically: even though the wrinkles still have a dominant orientation, some are buckled and some have other directions. Finally, deep into the "relaxed" phase (gray region in Fig. 3), the sheet can be in a vast number of metastable states [Fig. 1(a), left image], in contrast to the relatively small set of "bottleneck" states along the boundary. The well-defined phase space that can be repeatably accessed in our geometry may be useful in other investigations of metastable patterns in crumpled sheets, a topic of contemporary interest [21–24].

Equally striking is the difference among the possible paths from an arbitrary φ_ℓ with one set of ordered wrinkles, to $-\varphi_\ell$ with a mutually incompatible set. Uniquely, when one travels along the phase boundary the wrinkles deform smoothly as α changes, and they vanish momentarily at $\varphi_\ell=0$. All other paths traverse the bulk, compressing and buckling the initial wrinkles, and then straightening out the resulting network via many snap-through events—a noisy, messy, and highly path-dependent [24] journey that showcases the essential glassiness of a crumpled sheet.

We thank Ian Tobasco and Helen Ansell for informative discussions. This work was supported by NSF Awards DMR-CAREER-1654102 (P. D., M. H., J. D. P.) and DMR-2318680 (P. D., J D. P.).

- *keim@psu.edu †jdpaulse@syr.edu
- [1] Andrew Lennon and Sergio Pellegrino, in *Proceedings of the European Conference Spacecraft Structures, Materials & Mechanical Testing, Noordwijk, The Netherlands*, edited by Karen Fletcher (ESA, Noordwijk, The Netherlands, 2005), p. 101.
- [2] Joseph D. Paulsen, Wrapping liquids, solids, and gases in thin sheets, Annu. Rev. Condens. Matter Phys. **10**, 431 (2019).
- [3] Hervé Elettro, Sébastien Neukirch, Fritz Vollrath, and Arnaud Antkowiak, In-drop capillary spooling of spider capture thread inspires hybrid fibers with mixed solid-liquid mechanical properties, Proc. Natl. Acad. Sci. U.S.A. 113, 6143 (2016).
- [4] Paul Grandgeorge, Natacha Krins, Aurélie Hourlier-Fargette, Christel Laberty-Robert, Sébastien Neukirch, and Arnaud Antkowiak, Capillarity-induced folds fuel extreme shape changes in thin wicked membranes, Science **360**, 296 (2018).
- [5] Y. C. Fung, Elasticity of soft tissues in simple elongation, Am. J. Physiol.-Legacy Content **213**, 1532 (1967).

- [6] Ian Tobasco, Yousra Timounay, Desislava Todorova, Graham C. Leggat, Joseph D. Paulsen, and Eleni Katifori, Exact solutions for the wrinkle patterns of confined elastic shells, Nat. Phys. 18, 1099 (2022).
- [7] William Prager, On ideal locking materials, Trans. Soc. Rheol. 1, 169 (1957).
- [8] William Prager, On the formulation of constitutive equations for living soft tissues, Q. Appl. Math. 27, 128 (1969).
- [9] Herbert Wagner, Ebene Blechwandtrager mit sehr dunnem Stegblech (metal beams with very thin webs), Z. Flugtech. Motorloftschiffahr 20 (1929).
- [10] Allen C. Pipkin, The relaxed energy density for isotropic elastic membranes, IMA J. Appl. Math. 36, 85 (1986).
- [11] Eric Harold Mansfield, *The Bending and Stretching of Plates* (Cambridge University Press, Cambridge, 1989).
- [12] D. J. Steigmann and Albert Edward Green, Tension-field theory, Proc. R. Soc. A 429, 141 (1990).
- [13] Katia Bertoldi, Vincenzo Vitelli, Johan Christensen, and Martin Van Hecke, Flexible mechanical metamaterials, Nat. Rev. Mater. 2, 17066 (2017).
- [14] David Hilbert and Stephan Cohn-Vossen, Geometry and the Imagination (American Mathematical Society, Providence, 2021), Vol. 87.
- [15] Hugo Steinhaus, Mathematical Snapshots (Third American Edition Revised and Enlarged) (Oxford University Press, 1969).
- [16] Alfred Gray, Elsa Abbena, and Simon Salamon, *Modern Differential Geometry of Curves and Surfaces with Mathematica*® (Chapman and Hall/CRC, London, 2017).
- [17] See Supplemental Material at http://link.aps.org/supplemental/10.1103/PhysRevLett.131.148201 for supplementary figures, methods, and calculations.
- [18] R. J. Tait, D. J. Steigmann, and J. L. Zhong, Finite twist and extension of a cylindrical elastic membrane, Acta Mech. 117, 129 (1996).
- [19] Yu-Chuan Cheng, Ting-Heng Hsieh, Jih-Chiang Tsai, and Tzay-Ming Hong, Phase diagram and snap-off transition for twisted party balloons, Phys. Rev. E 104, 045004 (2021).
- [20] Julien Chopin and Arshad Kudrolli, Tensional twist-folding of sheets into multilayered scrolled yarns, Sci. Adv. 8, eabi8818 (2022).
- [21] Andrew B Croll, Timothy Twohig, and Theresa Elder, The compressive strength of crumpled matter, Nat. Commun. 10, 1502 (2019).
- [22] Yousra Timounay, Raj De, Jessica L. Stelzel, Zachariah S. Schrecengost, Monica M. Ripp, and Joseph D. Paulsen, Crumples as a Generic Stress-Focusing Instability in Confined Sheets, Phys. Rev. X 10, 021008 (2020).
- [23] Jovana Andrejevic, Lisa M. Lee, Shmuel M. Rubinstein, and Chris H. Rycroft, A model for the fragmentation kinetics of crumpled thin sheets, Nat. Commun. 12, 1470 (2021).
- [24] Dor Shohat, Daniel Hexner, and Yoav Lahini, Memory from coupled instabilities in unfolded crumpled sheets, Proc. Natl. Acad. Sci. U.S.A. 119, e2200028119 (2022).